

# Piezoelectrically actuated insect scale flapping wing

Sujoy Mukherjee\* and Ranjan Ganguli†

Department of Aerospace Engineering, Indian Institute of Science, Bangalore-560012, India

## ABSTRACT

An energy method is used in order to derive the non-linear equations of motion of a smart flapping wing. Flapping wing is actuated from the root by a PZT unimorph in the piezofan configuration. Dynamic characteristics of the wing, having the same size as dragonfly *Aeshna Multicolor*, are analyzed using numerical simulations. It is shown that flapping angle variations of the smart flapping wing are similar to the actual dragonfly wing for a specific feasible voltage. An unsteady aerodynamic model based on modified strip theory is used to obtain the aerodynamic forces. It is found that the smart wing generates sufficient lift to support its own weight and carry a small payload. It is therefore a potential candidate for flapping wing of micro air vehicles.

**Keywords:** Piezofan, non-linear vibrations, aerodynamics, flapping, MAV

## 1. INTRODUCTION

Recently, there has been a serious effort to design a class of very small flight vehicles called Micro Air Vehicles (MAVs) as their applications range from the military, surveillance in restricted spaces, planetary exploration, search-and-rescue to many more.<sup>1</sup> Essential requirements of such vehicles are power efficiency, high maneuverability and low-speed flight. Nature provides flapping flyers such as birds and insects which represent a very successful design for intelligent MAVs with much better performance than conventional wings and rotors.<sup>2</sup> Hence, birds and insects serve as a natural source of inspiration for the development of MAV. For a flapping-wing MAV, the wings are not only responsible for lift, but also for propulsion and maneuvers. Therefore, MAV flapping wing design represents one of the major challenges to efficient flight in the low Reynolds-number regime.

Biomimetic flapping wing mechanisms are used to achieve a deeper insight as well as qualitative and quantitative comprehension of flapping flight. VandenBerg and Ellington<sup>3</sup> made a scaled up robotic insect (the 'flapper') to mimic the complex movements of the wings of a hovering hawkmoth. It consists of two wings: a body which houses four d. c. servo motors and an elaborate gearbox to drive the wing movements. Dickinson et al.<sup>4</sup> built a dynamically scaled model of the fruit fly, *Drosophila melanogaster*. The motion of the two wings is driven by an assembly of six computer-controlled stepper motors attached to the wing gearbox via timing belts and coaxial drive shafts. Tarascio et al.<sup>5</sup> developed a mechanism which is an insect-based flapping wing, passive pitch, bistable device that is capable of replicating the complex kinematics of insect wings in hover. The desired flapping and pitching motion was generated by a brushless motor, the speed of which was controlled by a sensorless speed controller in combination with a precision pulse generator. Yamamoto and Isogai<sup>6</sup> developed a mechanical flapping wing apparatus that dynamically simulates the tandem wing configuration of a dragonfly in hovering flight. The flapping and feathering motion are induced by electric sliders and stepping motors, respectively. In a recent study, Singh and Chopra<sup>7</sup> investigated the aeroelastic effects associated with the lightweight and highly flexible wing using a biomimetic flapping mechanism. They showed that wing flexibility plays a key role in the thrust generating capability of MAV scale flapping wings. It can be noted from the above studies that biomimetic flapping wing mechanisms have very important contributions in the fundamental understanding of the flapping flight. However, these dynamically scaled flapping wing mechanisms may not be suitable for use in small or micro-scale flying vehicles as they are bulky and flap at very low frequency. Moreover, current flapping wing mechanisms rely on pneumatic and motor-driven flapping actuators which lead to high weight and system-complexity.<sup>8</sup> Natural flapping flyers generate lift and thrust using complex wingbeat kinematics which can not be easily mimicked with these conventional actuators. Another plausible alternative may be to use actuator made of smart materials.

\* PhD Student; sujoy@aero.iisc.ernet.in

† Professor; Phone: +91-080-2293-3017/2438; ganguli@aero.iisc.ernet.in

Smart materials, especially piezoelectric materials, are widely used in smart structures as sensors and actuators because they have several attractive features such as high bandwidth, high output force, compact size and high power density.<sup>9</sup> Cox et al.<sup>10</sup> used PZT unimorph actuators for developing three four-bar and five-bar linkage flapping mechanisms to mechanically emulate flapping flight on the meso-scale. Sitti<sup>11</sup> used piezoelectric unimorph actuators to develop four-bar mechanisms for micromechanical flying insect thorax. In a recent work, Nguyen et al.<sup>12</sup> used in their experiment a unimorph piezoceramic actuator called a lightweight piezocomposite actuator (LIPCA) in the simply supported configuration to actuate insect-mimicking flapping system which is a four-bar linkage system. Kim et al.<sup>13</sup> also used in their experiment micro-fiber composite (MFC) actuator to generate an adaptive camber motion which produces sufficient aerodynamic benefit. It can be noted from these works that some kind of motion amplification mechanisms are necessary in order to obtain large deflection because the piezoelectric effect is intrinsically small and leads to a small deflection when expected directly from the bending piezoelectric unimorph/bimorph.<sup>14</sup>

Piezoelectric fan (piezofan), which was first proposed by Toda and Osaka,<sup>15</sup> is one of the simple motion amplifying mechanisms. Piezofan couples a piezoelectric unimorph to an attached flexible wing and is competent to produce large deflection, as high as  $47^\circ$ , especially at resonance.<sup>16</sup> Piezoelectric fans are popular as a very compact, low power, noiseless air cooling technology for portable electronic devices such as cellular phones, DVD players, laptop computers etc.<sup>17</sup> Chung et al.<sup>8</sup> used two coupled piezofans in parallel driven by sinusoidal voltages with different phase delay between them to control the flapping and twisting motions of the wing. Their experimental investigation showed that the bending amplitude of the wing reduced with the increasing phase delay and the twisting movement increased with an increasing phase delay. In another study, Chung et al.<sup>14</sup> proposed a form of design optimization using the Strouhal number and a limited numbers of materials parameters to select the best piezofans for flapping wing MAV applications. They used linear analytical model to analyze the performance of piezofan structure at dynamic operation. However, the wings of birds and insects move through a large angle which may be obtained using piezofan through large deflection. Therefore, non-linear dynamic model is needed to perform dynamic analysis. Mahmoodi and Jalili<sup>18</sup> derived the non-linear equations of motion of a non-homogenous piezoelectrically actuated microcantilever beam. The non-linear terms appeared in the form of quadratic expression due to presence of piezoelectric layer, and cubic form due to geometrical non-linearities. In order to consider the piezofan for flapping wing applications, it is necessary to analyze its aerodynamic performance. Hence, aerodynamic model is needed for obtaining the aerodynamic forces.

Aerodynamic models used for the flapping wing flight can be broadly classified into quasi-steady models and unsteady models. The quasi-steady models assume low flapping frequencies so that shed wake effects are negligible.<sup>19</sup> In the unsteady models, unsteady aerodynamic characteristics are accounted for by the unsteady wake effects.<sup>20</sup> Selected researchers have used computational fluid dynamics (CFD) to simulate the flapping flight.<sup>21,22</sup> CFD methods provide a clear picture of the flow by solving the incompressible form of the Navier-Stokes equations. However, CFD simulations are computationally intensive. DeLaurier<sup>20</sup> proposed an unsteady aerodynamic model based on modified strip theory. The aerodynamic model makes it possible to estimate the aerodynamic performances of harmonically flapping wings in the phase of preliminary design and development.<sup>23</sup> Various aerodynamic effects can be considered in this model such as camber effect, partial leading edge suction effect, viscous effect, unsteady wake effect and dynamic stall model of pitching motion. Therefore, the DeLaurier model is useful for estimating the lift generated by a flapping wing.

In this paper, an energy method is used in order to derive the non-linear equations of motion of a smart flapping wing. Flapping wing is actuated from the root by a PZT unimorph in the piezofan configuration. Dynamic characteristics of the wing, having the same size as dragonfly *Aeshna Multicolor*, are analyzed using numerical simulations. Flapping angle variations of the smart flapping wing is compared with experimental data of the actual dragonfly wing. Experimental data of flapping angle variations of actual dragonfly wing is obtained from literature. Finally, an unsteady aerodynamic model based on modified strip theory is used to obtain the aerodynamic forces.

## 2. STRUCTURAL MODEL

Fig. 1 shows the schematic diagram of the flapping wing where a piezoelectric unimorph is attached to the uniform flexible wing. Piezoelectric unimorph is utilized to actuate the wing by supplying a voltage,  $P_e(t)$ .

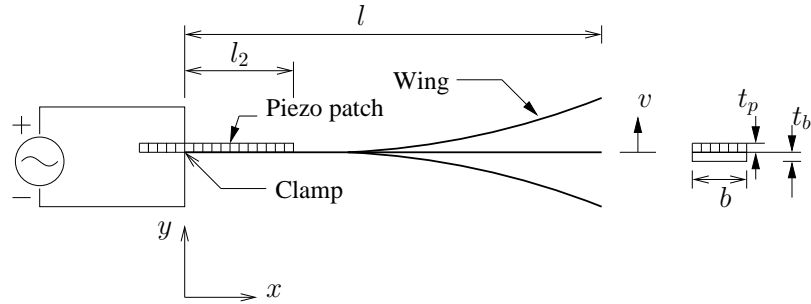


Figure 1. Schematic of the piezoelectrically actuated flapping wing.

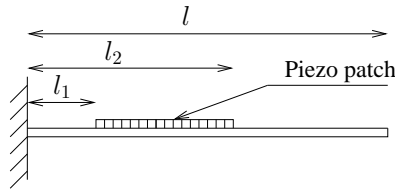


Figure 2. Schematic diagram of flapping wing geometry used for modeling.

Schematic diagram of the wing geometry used for the structural modeling is shown in Fig. 2. Fig. 3 shows a wing segment of length  $s$ . To describe the dynamics of the wing, two coordinate systems are utilized: the  $(x, y, z)$  system is considered to be inertial and the  $(\xi, \tilde{\theta}, \zeta)$  system is local principal system.<sup>18</sup> The relationship between the principal and the inertial coordinates is described by the Euler rotation  $\psi(s, t)$ . Using Fig. 3, angle  $\psi(s, t)$  for an element of length  $ds$  can be written as

$$\psi = \tan^{-1} \frac{v'}{1 + u'} \quad (1)$$

where the over prime denotes derivative with respect to the arc length. The longitudinal and transverse displacements are described by  $u(s, t)$  and  $v(s, t)$ , respectively. Utilizing Green's strain theory, strain of the neutral axis ( $\varepsilon_0$ ) is given by<sup>24</sup>

$$\varepsilon_0 = \sqrt{(1 + u'^2) + v'^2} - 1 \quad (2)$$

Longitudinal and bending vibration can be related using inextensibility condition which demands no relative elongation of the neutral axis. Using the Taylor series expansion, Equation (2) reduces to

$$u' = -\frac{1}{2}v'^2 \quad (3)$$

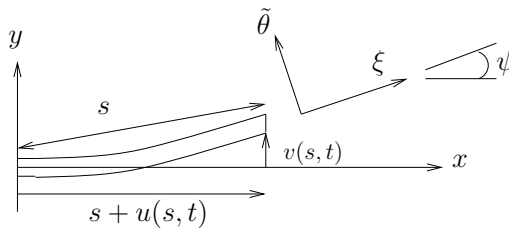


Figure 3. Principal and inertial coordinate systems.

The piezoelectric layer is not attached to the entire length of the wing. Therefore, the neutral surface,  $y_n$ , changes for each section and can be obtained as

$$y_n = \begin{cases} 0, & s < l_1 \text{ or } s > l_2 \\ \frac{E_p t_p (t_p + t_b)}{2(E_p t_p + E_b t_b)}, & l_1 < s < l_2 \end{cases} \quad (4)$$

The equations of motions are derived using an energy method.<sup>18</sup> The total kinetic energy ( $\mathcal{T}$ ) of the system can be expressed as

$$\mathcal{T} = \frac{1}{2} \int_0^l (m(s)(\dot{u}^2 + \dot{v}^2) + J(s)(\dot{v}'^2 - 2\dot{v}'^2 u' - 2v' \dot{u}' \dot{v}' - 2\dot{v}'^2 v'^2)) ds \quad (5)$$

where

$$m(s) = b(\rho_b t_b + (H_{l_1} - H_{l_2})\rho_p t_p) \quad (6)$$

Here,  $H(s)$  is the Heaviside function and  $J(s)$  is the mass moment of inertia of the wing. Similarly, the total potential energy ( $\mathcal{V}$ ) of the system can be written as

$$\begin{aligned} \mathcal{V} = & \frac{1}{2} \int_0^{l_1} \int \int_A \sigma_{11}^b \varepsilon_{11}^b dA ds + \frac{1}{2} \int_{l_1}^{l_2} \int \int_A \sigma_{11}^b \varepsilon_{11}^b dA ds + \frac{1}{2} \int_{l_1}^{l_2} \int \int_A (\sigma_{11}^p \varepsilon_{11}^p + Q_2 D_2) dA ds \\ & + \frac{1}{2} \int_{l_1}^{l_2} \int \int_A \sigma_{11}^b \varepsilon_{11}^b dA ds + \frac{1}{2} \int_0^l EA(s) \left( u'^2 + u' v'^2 + \frac{1}{4} v'^4 \right) ds \end{aligned} \quad (7)$$

The following fundamental assumptions are made for the analysis:

1. The wing is initially straight and it is clamped at one end and free at other end,
2. The Euler-Bernoulli beam theories are followed, where shear deformation and rotary inertia terms are negligible,
3. The wing is inextensible,
4. Both, the piezoelectric layer and the wing have same width, and
5. Bonding layer is assumed to be perfect.

Considering all the assumptions and applying the extended Hamilton's principle, governing equations of motion can be obtained as

$$\begin{aligned} m(s)\ddot{v} + \frac{\partial^2}{\partial s^2} (C_\zeta(s)v'') + \frac{\partial}{\partial s} \left[ v' \int_l^s m(s) \int_0^s (\ddot{v}' + \dot{v}'^2) ds ds \right] + \left[ v' \frac{\partial^2}{\partial s^2} (C_\zeta(s)v''v') + v'' \frac{\partial}{\partial s} (C_\zeta(s)v''v') \right] \\ v' \frac{\partial}{\partial s} \left[ \frac{C_d^2(s)}{C_\beta(s)} v''v' - \frac{bC_c(s)}{C_\beta(s)} P_e(t)v' \right] - \frac{\partial^2}{\partial s^2} \left[ \frac{bC_d(s)}{C_\beta(s)} P_e(t) \left( 1 - \frac{1}{2}v'^2 \right) + \frac{C_d^2(s)}{C_\beta(s)} v'' \right] = 0 \end{aligned} \quad (8)$$

with the boundary conditions

$$v(0, t) = v'(0, t) = v''(l, t) = v'''(l, t) = 0 \quad (9)$$

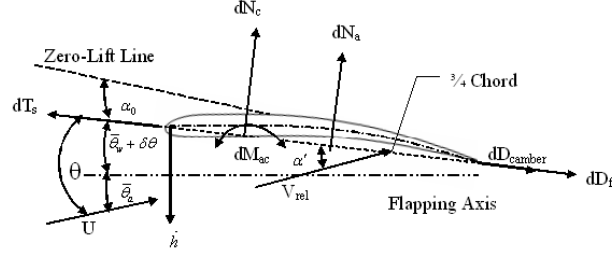


Figure 4. Aerodynamic forces and motion variables of a wing section.

Cubic non-linear terms of inertia and stiffness, resulting from the geometry of the vibrating wing, appear in the equations of motion. Moreover, coupling of electrical and mechanical fields introduces quadratic and cubic nonlinearities due to piezoelectric effect. The Galerkin method is utilized to discretize the system as

$$v(s, t) = \sum_{n=1}^{\infty} v_n(s, t) = \sum_{n=1}^{\infty} \phi_n(s) q_n(t) \quad (10)$$

where  $\phi_n$  are companion functions and  $q_n$  are generalized time-dependent coordinates. In order to solve the equations of motion utilizing the method of multiple scales,<sup>25</sup> Equation (8) is rewritten in the form:

$$\ddot{q}_n + \varepsilon \mu \dot{q}_n + \omega_n^2 q_n + \varepsilon^2 k_{1n} f(t) q_n^2 + \varepsilon k_{2n} q_n^3 + \varepsilon k_{3n} (q_n^2 \ddot{q}_n + q_n \dot{q}_n^2) + \varepsilon k_{4n} f(t) = 0 \quad (11)$$

Now,  $q_n(t)$  can be expressed by order of  $\varepsilon$  as<sup>26</sup>

$$q_n(t; \varepsilon) = q_{0n}(T_0, T_1) + \varepsilon q_{1n}(T_0, T_1) + \dots \quad (12)$$

where,  $T_0$  and  $T_1$  are the time scales. Frequency response of the system can be expressed as

$$\left( \frac{1}{2} \mu \omega_n a_n \right)^2 + \left( \frac{3}{8} k_{2n} a_n^3 - \omega_n^2 \sigma a_n \right)^2 = k_{4n}^2 f^2 \quad (13)$$

where  $\sigma$  is a detuning parameter and  $a_n$  is the amplitude of the generalized coordinate  $q_n(t)$ . Finally, the deflection at the tip of the wing is obtained by

$$v(l, t) = \phi_n(l) a_n(t) \cos(\beta_n t + \beta_0) = \phi(l) q(t) \quad (14)$$

### 3. AERODYNAMIC MODEL

The aerodynamic model is based on the modified strip theory as proposed by DeLaurier,<sup>20</sup> in which the aerodynamic forces of the flapping wing are obtained by integrating the sectional aerodynamic forces calculated in each section. In this unsteady aerodynamic model, the kinematics for a section of the wing is represented by a plunging velocity  $\dot{h}$  and a pitch angle of the chord  $\theta$  relative to the free stream velocity, as shown in Fig. 4.<sup>20</sup> The local parameters determining the forces includes the section's geometry, relative angle of attack at the  $\frac{3}{4}$ -chord location, pitch rates and the dynamic pressure at the  $\frac{1}{4}$ -chord location. The aerodynamic forces acting on each section of the wing are divided into the normal force  $dN$ , and the chordwise force,  $dF_X$ . The components of the normal force are: (i)  $dN_c$ , a circulatory force normal to the chord at the  $\frac{1}{4}$ -chord location and (ii)  $dN_a$ , an apparent-mass force normal to the chord at the  $\frac{1}{2}$ -chord location. The expressions for the normal force components are as follows:

$$dN_c = \frac{\rho_{air} U V}{2} C_n c dy \quad (15)$$

$$dN_a = \frac{\rho_{air}\pi c^2}{4} \dot{v}_2 dy \quad (16)$$

Therefore, the section's total attached flow normal force is

$$dN = dN_c + dN_a \quad (17)$$

The components of the chordwise force are: (i)  $dT_s$ , a chordwise leading edge suction force, (ii)  $dD_{camber}$ , a chordwise drag due to camber, and (iii)  $dD_f$ , a chordwise drag due to skin friction. The expressions for the chordwise force components are as follows:

$$dT_s = \eta_s 2\pi \left( \alpha' + \bar{\theta}_a - \frac{c\dot{\theta}}{4U} \right)^2 \frac{\rho_{air}UV}{2} c dy \quad (18)$$

$$dD_{camber} = -2\pi\alpha_0 (\alpha' + \bar{\theta}_a + \bar{\theta}_w) \frac{\rho_{air}UV}{2} c dy \quad (19)$$

$$dD_f = (C_d)_f \frac{\rho_{air}V_x^2}{2} c dy \quad (20)$$

Thus, the total chordwise force is

$$dF_X = dT_s - dD_{camber} - dD_f \quad (21)$$

The equations for the segment's instantaneous lift  $dL$  and thrust  $dT$  are

$$dL = dN \cos \theta + dF_X \sin \theta \quad (22)$$

$$dT = dF_X \cos \theta - dN \sin \theta \quad (23)$$

These may be integrated along the span to give the whole wing's instantaneous lift and thrust:

$$L(t) = 2 \int_0^{\frac{b}{2}} \cos \gamma dL \quad (24)$$

$$T(t) = 2 \int_0^{\frac{b}{2}} dT \quad (25)$$

where  $\gamma(t)$  is the section's dihedral angle at that instant in the flapping cycle. The wing's average lift and thrust are obtained by integrating  $L(t)$  and  $T(t)$  over the cycle. Integrating with respect to cycle angle,  $\phi$ , instead of time,  $t$ , where

$$\phi = \omega t \quad (26)$$

so that the average lift and thrust are expressed as

$$\bar{L} = \frac{1}{2\pi} \int_0^{2\pi} L(\phi) d\phi \quad (27)$$

$$\bar{T} = \frac{1}{2\pi} \int_0^{2\pi} T(\phi) d\phi \quad (28)$$

The complete details of the aerodynamic model are given by DeLaurier.<sup>20</sup>

Table 1. Material and geometric properties used for model validation

Microcantilever beam		Piezoelectric layer	
Parameter	Value	Parameter	Value
Young's modulus	105 GPa	Young's modulus	104 GPa
Beam length	500 $\mu\text{m}$	Piezoelectric length	375 $\mu\text{m}$
Width	250 $\mu\text{m}$	Width	130 $\mu\text{m}$
Tip mass width	55 $\mu\text{m}$	Coupling co-efficient	500 MV/m
Poisson's ratio	0.28	Poisson's ratio	0.25
Density	2330 $\text{Kg/m}^3$	Density	6390 $\text{Kg/m}^3$
Thickness	4 $\mu\text{m}$	Thickness	4 $\mu\text{m}$

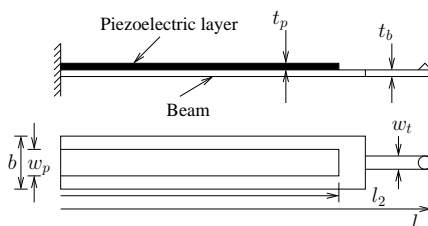


Figure 5. Geometry of the microcantilever beam.

#### 4. RESULTS AND DISCUSSION

In order to validate the dynamic model, numerical analysis is carried out for a structure which is used by Mahmoodi and Jalili<sup>18</sup> as shown in Fig. 5. The physical properties, used for this analysis, are given in the Table 1. Fig. 6 shows the tip deflection due to the excitation voltage of 0.5V. Excitation voltage is increased to 1.5V and the corresponding tip deflection is shown in Fig. 7. It can be seen from the Fig. 6 and Fig. 7 that tip deflection is sensitive to the input excitation voltage. Moreover, the results of this analysis match well with the results presented in Mahmoodi and Jalili.<sup>18</sup> Therefore, the model implementation is validated.

In the present study, the size of the flapping wing is chosen to an insect scale. Insects, such as the dragonfly, fly with unusual aerial agility. Dragonfly flight satisfies all the requirements of an MAV flight envelope therefore providing inspiration for MAV design. The length and width of the flapping wing, made of Mylar, are taken as 4 cm and 1 cm, respectively, which are typical values for the dragonfly *Aeshna Multicolor* wing.<sup>27</sup> Flapping wing is actuated from the root by a PZT unimorph in the piezofan configuration as shown in Fig. 1. Input excitation voltage is assumed to be harmonic to generate flapping motion. Material and geometric properties pertaining to the flapping wing is given in Table 2.

These properties are used to calculate tip deflections of the flapping wing. Fig. 8 shows the tip deflections of the flapping wing due to different input excitations. Since tip deflection is sensitive to the input excitation

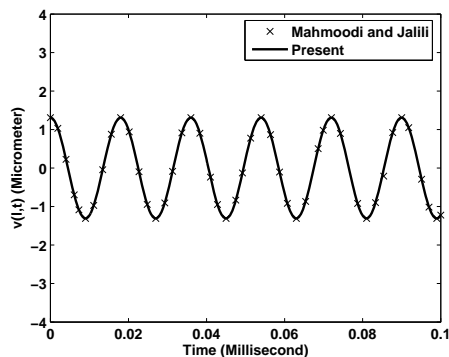


Figure 6. Tip deflection due to 0.5V excitation.

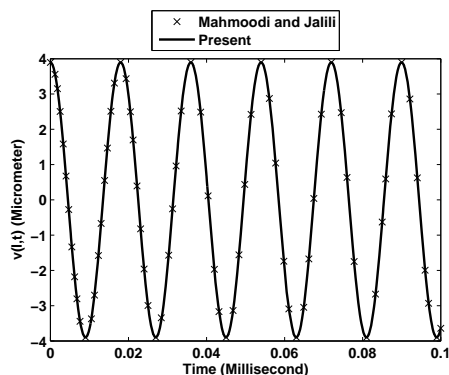


Figure 7. Tip deflection due to 1.5V excitation.

Table 2. Material and geometric properties of the flapping wing  
**Wing** **PZT 5H layer**

Parameter	Value <sup>17</sup>	Parameter	Value <sup>14</sup>
Young's modulus	4.6 GPa	Young's modulus	62 GPa
Wing length	40 mm	Piezoelectric length	10 mm
Width	10 mm	Width	10 mm
Thickness	200 $\mu\text{m}$	Thickness	200 $\mu\text{m}$
Density	1240 Kg/m <sup>3</sup>	Piezoelectric constant	$-320 \times 10^{-12}$ m/V
Poisson's ratio	0.44	Density	7800 Kg/m <sup>3</sup>
Mass	99.2 mg	Mass	156 mg

voltage, tip deflections increases with the increase of input excitation voltage. A tip deflection of 24 mm is obtained at 90 V and it reaches up to 27 mm at 120 V at 41 Hz. Flapping angle can be measured from the tip deflection following the procedure as explained schematically in Fig. 9. Flapping angle variation of the wing is shown in Fig. 10. It can be seen from the Fig. 10 that flapping angle of  $31^\circ$  is obtained at 90 V and it increases up to  $34^\circ$  at 120 V. Flapping angle which is obtained using the non-linear dynamic model, given in section 2, at 120 V belongs to non-linear regime. Flapping angle variations of the smart flapping wing is compared with the flapping angle variations of actual dragonfly wing as measured experimentally by Zeng et al.<sup>28</sup> Fig. 10 shows the tip motion of the smart flapping wing is similar to the actual dragonfly wing tip motion in the flapping mode. Here, the smart flapping wing is actuated at a frequency 41 Hz which is close to the flapping frequency, 32 Hz, of the actual dragonfly wing.<sup>28</sup> As mentioned earlier, it is necessary to analyze aerodynamic performance to consider the smart flapping wing for MAV applications.

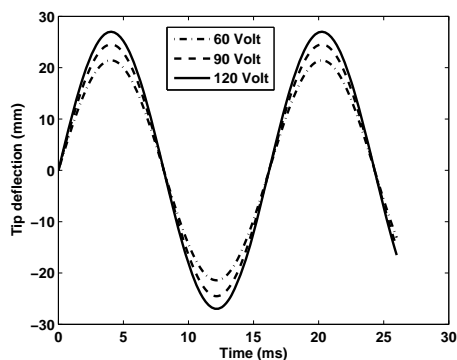


Figure 8. Tip deflection of the flapping wing due to application of different voltages.

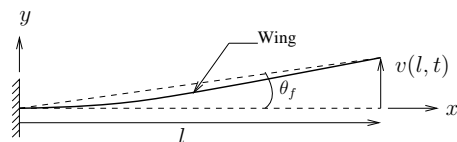


Figure 9. Schematic diagram of calculating flapping angle.

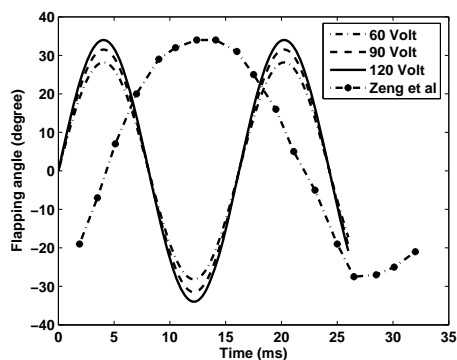


Figure 10. Comparison of flapping angle variations with experimental data.

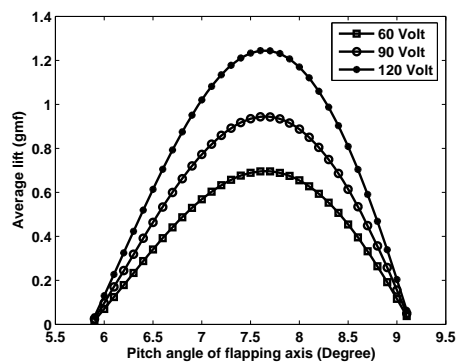


Figure 11. Average lift at different pitch angle.

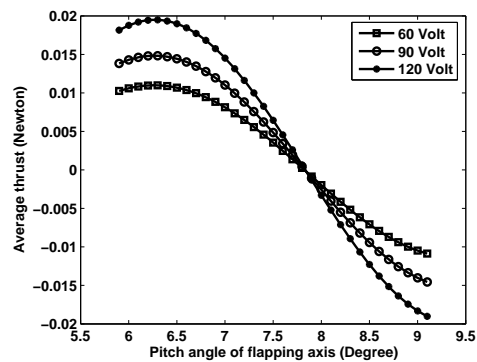


Figure 12. Average thrust at different pitch angle.

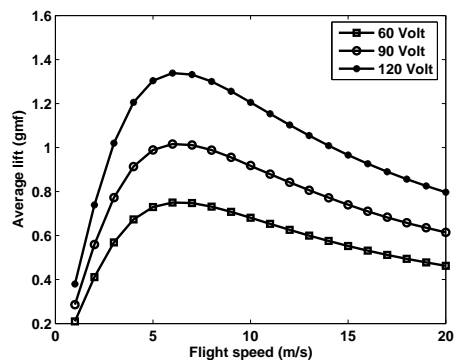


Figure 13. Average lift at different flight speed.

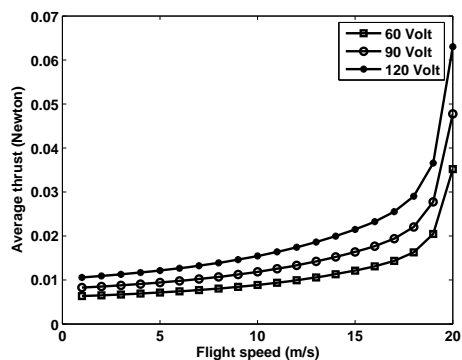


Figure 14. Average thrust at different flight speed.

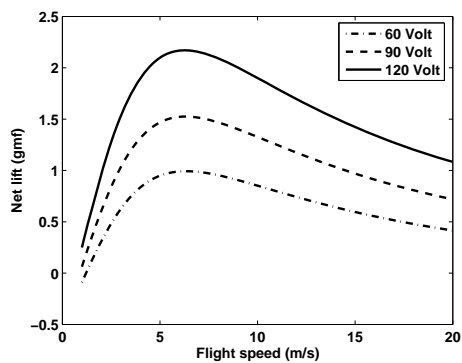


Figure 15. Net lift at different flight speed.

For aerodynamic modeling, kinematics pertaining to the wing section located at 75% of the wing span is considered for calculation of the aerodynamic forces. Selection of the pitch angle of the flapping axis  $\theta_a$ , as shown in Fig. 4, is important for the performance of the flapping wing. Average lift pertaining to single wing at different pitch angle is shown in Fig. 11 when different voltages are applied. Fig. 12 shows the average thrust at different pitch angle and at different applied voltages. It can be seen from the Fig. 11 that the lift is maximum at the pitch angle of  $7.8^\circ$ . However, at the pitch angle of  $7.8^\circ$ , thrust which is same for all the three applied voltages has a negative value. Since average thrust force must be positive to satisfy the condition for cruise flight, therefore the value of  $\theta_a$  is selected as  $7^\circ$ .

Fig. 13 shows the average lift produced by the smart flapping wing at different flight speeds. It can be seen from the Fig. 13 that maximum lift force of 1.02 g is obtained at 90 V. It can also be seen that the maximum lift force can reach up to 1.34 g at 120V. In both the cases, maximum lift force occurs at the flight speed of 6.2 m/s. Average thrust force at different flight speeds is shown in Fig. 14. The average thrust force is found to be 0.0128 N at the flight speed of 6.2 m/s when 120 V is applied. Fig. 15 shows the net lift force, obtained by subtracting the total wing weight from the total lift force, when two smart flapping wings are used. It can be seen from the Fig. 15 that flapping wings can carry a payload of 2.17 g at 120 V. They are therefore a prospective candidate for flapping wing MAVs at insect scales.

In order to be capable of autonomous flight, the flapping wing MAV requires several sub-systems such as power supply unit, control unit, sensory systems etc. These sub-systems can be made of light weight components such as thin sheet of solar cell may be used for power supply unit.<sup>29,30</sup> The net lift force generated by the smart flapping wing may be used to carry one or more of these sub-systems.

## 5. CONCLUSIONS

In this study, an energy method is used in order to derive the non-linear equations of motion of a smart flapping wing. Flapping wing is actuated from the root by a PZT unimorph in the piezofan configuration. Dynamic characteristics of the wing, having the same size as dragonfly *Aeshna Multicolor*, are analyzed using numerical simulations. A flapping angle of  $31^\circ$  is obtained at 90 V. It is possible to produce a flapping angle of  $34^\circ$  when the input excitation voltage is 120 V at 41 Hz. Therefore, it can produce same flapping angle variation as an actual dragonfly wing. An unsteady aerodynamic model is used to obtain the aerodynamic forces. The smart flapping wing can generate 1.34 g average lift force at the flight speed of 6.2 m/s when driven by sinusoidal voltage of 120 V at 41 Hz. The average thrust is found to be 0.0128 N at the same flight conditions. Moreover, it is possible to carry a payload of 2.17 g by using a pair of smart flapping wings actuated at 120 V, 41 Hz and flying at 6.2 m/s. The smart flapping wing based on the piezofan concept may be considered as a potential candidate for use in MAV applications.

## REFERENCES

- [1] Rosenfeld, N. C. and Wereley, N. M., "Time-periodic stability of a flapping insect wing structure in hover," *Journal of Aircraft* **46(2)**, 450–464 (2009).
- [2] Ansari, S. A., Zbikowski, R., and Knowles, K., "Aerodynamic modelling of insect-like flapping flight for micro air vehicles," *Progress in Aerospace Sciences* **42(2)**, 129–172 (2006).
- [3] VandenBerg, C. and Ellington, C. P., "The vortex wake of a 'hovering' model hawkmoth," *Philosophical Transactions of the Royal Society of London Series B-Biological Sciences* **352(1351)**, 317–328 (1997).
- [4] Dickinson, M. H., Lehmann, F. O., and Sane, S. P., "Wing rotation and the aerodynamic basis of insect flight," *Science* **284(5422)**, 1954–1960 (1999).
- [5] Tarascio, M. J., Ramasamy, M., Chopra, I., and Leishman, J. G., "Flow visualization of micro air vehicle scaled insect-based flapping wings," *Journal of Aircraft* **42(2)**, 385–390 (2005).
- [6] Yamamoto, M. and Isogai, K., "Measurement of unsteady fluid dynamics forces for a mechanical dragonfly model," *AIAA Journal* **43(12)**, 2475–2480 (2005).
- [7] Singh, B. and Chopra, I., "Insect-based hover-capable flapping wings for micro air vehicles: experiments and analysis," *AIAA Journal* **46(9)**, 2115–2135 (2008).

- [8] Chung, H. C., Kummari, K. L., Croucher, S. J., Lawson, N., Guo, S., and Huang, Z., "Coupled piezoelectric fans with two degree of freedom motion for the application of flapping wing micro aerial vehicles," *Sensors and Actuators A - Physical* **147(2)**, 607–612 (2008).
- [9] Chopra, I., "Review of state of art of smart structures and integrated systems," *AIAA Journal* **40(11)**, 2145–2187 (2002).
- [10] Cox, A., Monopoli, D., Cveticanin, D., Goldfarb, M., and Garcia, E., "The development of elastodynamic components for piezoelectrically actuated flapping micro-air vehicles," *Journal of Intelligent Material Systems and Structures* **13(9)**, 611–615 (2002).
- [11] Sitti, M., "Piezoelectrically actuated four-bar mechanism with two flexible links for micromechanical flying insect thorax," *IEEE-ASME Transactions on Mechatronics* **8(1)**, 26–36 (2003).
- [12] Nguyen, V. Q., Syaifuddin, M., Park, H. C., Byun, D. Y., Goo, N. S., and Yoon, K. J., "Characteristics of an insect-mimicking flapping system actuated by a unimorph piezoceramic actuator," *Journal of Intelligent Material Systems and Structures* **19(10)**, 1185–1193 (2008).
- [13] Kim, D. K., Kim, H. I., Han, J. H., and Kwon, K. J., "Experimental investigation on the aerodynamic characteristics of a bio-mimetic flapping wing with macro-fiber composites," *Journal of Intelligent Material Systems and Structures* **19(3)**, 423–431 (2008).
- [14] Chung, H. C., Kummari, K. L., Croucher, S. J., Lawson, N., Guo, S., Whatmore, R. W., and Huang, Z., "Development of piezoelectric fans for flapping wing application," *Sensors and Actuators A - Physical* **149(1)**, 136–142 (2009).
- [15] Toda, M. and Osaka, S., "Vibrational fan using the piezoelectric polymer PVF<sub>2</sub>," *Proceedings of the IEEE* **67(8)**, 1171–1173 (1979).
- [16] Yao, K. and Uchino, K. J., "Analysis on a composite cantilever beam coupling a piezoelectric bimorph to an elastic blade," *Sensors and Actuators A - Physical* **89(3)**, 215–221 (2001).
- [17] Wait, S. M., Basak, S., Garimella, S. V., and Raman, A., "Piezoelectric fans using higher flexural modes for electronics cooling applications," *IEEE Transactions on Components and Packaging Technologies* **30(1)**, 119–128 (2007).
- [18] Mahmoodi, S. N. and Jalili, N., "Non-linear vibrations and frequency response analysis of piezoelectrically driven microcantilevers," *International Journal of Non-Linear Mechanics* **42(4)**, 577–587 (2007).
- [19] Betteridge, D. S. and Archer, R. D., "A study of the mechanics of flapping wings," *Aeronautical Quarterly* **25**, 129–142 (1974).
- [20] DeLaurier, J. D., "An aerodynamic model for flapping-wing flight," *Aeronautical Journal* **97(964)**, 125–130 (1993).
- [21] Wang, Z. J., "Vortex shedding and frequency selection in flapping flight," *Journal of Fluid Mechanics* **410**, 323–341 (2000).
- [22] Wu, J. H. and Sun, M., "Unsteady aerodynamic forces of a flapping wing," *Journal of Experimental Biology* **207(23)**, 1137–1150 (2004).
- [23] Ke, S., Zhigang, W., and Chao, Y., "Analysis and flexible structural modeling for oscillating wing utilizing aeroelasticity," *Chinese Journal of Aeronautics* **21(5)**, 402–410 (2008).
- [24] Hsieh, S. R., Shaw, S. W., and Pierre, C., "Normal modes for large amplitude vibration of a cantilever beam," *International Journal of Solids and Structures* **31(40)**, 1981–2014 (1994).
- [25] Nayfeh, A. H. and Mook, D. T., [*Nonlinear Oscillations*], Wiley, New York (1979).
- [26] Nayfeh, A. H., [*Perturbation Methods*], Wiley, New York (1973).
- [27] Combes, S. A. and Daniel, T. L., "Flexural stiffness in insect wings ii. spatial distribution and dynamic wing bending," *Journal of Experimental Biology* **206(17)**, 2989–2997 (2003).
- [28] Zeng, L., Matsumoto, H., and Kawachi, K., "A fringe shadow method for measuring flapping angle and torsional angle of a dragonfly wing," *Measurement Science and Technology* **7(5)**, 776–781 (1996).
- [29] Deng, X., Schenato, L., Wu, W. C., and Sastry, S. S., "Flapping flight for biomimetic robotic insects: part i - system modeling," *IEEE Transactions On Robotics* **22(4)**, 776–788 (2006).
- [30] Tanaka, K., Oonuki, M., Moritake, N., and Uchiki, H., "Cu<sub>2</sub>ZnSnS<sub>4</sub> thin film solar cells prepared by non-vacuum processing," *Solar Energy Materials and Solar Cells* **93(5)**, 583–587 (2009).